Entrapment and rigidification of adenine by a photo-cross-linked thymine network leads to fluorescent polymer nanoparticles

Hua, Z.; Wilks, T.R.; Keogh, R.; Herwig, G.; Stavros, V.G.; O'Reilly, R.K.

DOI:
10.1021/acs.chemmater.7b05206

Document Version
Peer reviewed version

Citation for published version (Harvard):
Hua, Z, Wilks, TR, Keogh, R, Herwig, G, Stavros, VG & O'Reilly, RK 2018, 'Entrapment and rigidification of adenine by a photo-cross-linked thymine network leads to fluorescent polymer nanoparticles', *Chemistry of Materials*, vol. 30, no. 4, pp. 1408-1416. https://doi.org/10.1021/acs.chemmater.7b05206

Entrapment and Rigidification of Adenine by a Photocrosslinked Thymine Network Leads to Fluorescent Polymer Nanoparticles

Zan Hua, Thomas R. Wilks, Robert Keogh, Gordon Herwig, Vasilios G. Stavros and Rachel K. O'Reilly*

Department of Chemistry, University of Warwick, Gibbet Hill Road, Coventry, CV4 7AL, UK.

ABSTRACT: Photocrosslinking of nucleobase-containing polymer micelles was observed to result in fluorescent polymer nanoparticles. By varying the micelle assembly conditions, it was possible to probe the origins of this behavior. A number of factors were investigated including the effect of omitting one of the nucleobases, blocking hydrogen-bonding interactions, detaching the nucleobase from the polymer backbone and changing the degree of core crosslinking. Spectroscopic investigations were also carried out to further characterize the fluorescent nanoparticles. These data revealed that no new small molecule fluorophores were created during crosslinking and that a dense, hydrogen-bonded network of photodimerized thymine with entrapped adenine was required for fluorescence to arise. We conclude that rigidification and immobilization of adenine in this way leads to the enhancement of an already extant fluorescence pathway, and suggests that synergistic covalent and supramolecular entrapment of profluorophores may provide a general strategy for the production of novel fluorescent polymer nanoparticles.

Introduction

Highly specific hydrogen-bonding (H-bonding) interactions between complementary nucleobases form the basis of nature's ability to encode genetic information in the DNA double helix and enable the essential biological functions of transcription, translation and replication. Inspired by this selective recognition, synthetic chemists have widely utilized complementary H-bonding interactions to achieve templated polymerization/synthesis,[1–6] fabricate DNA-like supramolecular aggregates,[7] and tune nanostructure morphologies and functionalities.[8–12]

Thymine, one of the natural nucleobases, can undergo photodimerization under UV irradiation to generate a cyclobutane pyrimidine,[13,14] and this has been exploited by various groups, for example in the fabrication of adhesive materials[15] and the formation of core-crosslinked polymer nanoparticles.[16] Photodimerization is an attractive crosslinking method as it is non-toxic, tunable, controllable remotely and does not yield any byproducts.[17] Our laboratory has recently reported the synthesis of a new class of nucleobase-containing nanoparticles based on diblock copolymers containing adenine (A) or thymine (T).[5,9,10,18,19] Polymers with relatively long nucleobase blocks self-assemble in water to give micelles with an A or T core. When a diblock copolymer with the complementary nucleobase is added it is absorbed, driven by A:T base pairing in the micelle core. This behavior can be exploited to various ends. For example, varying the A:T ratio and polymer block lengths resulted in highly tunable switching of the micelle size and shape.[9] More recently, we have shown that by attaching different hydrophilic blocks to the A- and T-containing polymers it is possible to create micelles with a mixed polymer corona, and to straightforwardly introduce different functional groups (such as protein ligands) with a high degree of control over loading density.[10] However, the above systems are not stable to dilution or to changes in solvent since the micelles are held together solely by supramolecular interactions in the core.

Inspired by the work described above, we wanted to explore whether photodimerization of T could be used as a straightforward method for the core crosslinking of nucleobase-containing micelles. Interestingly, our initial experiments revealed that at high crosslinking densities the A:T-containing nanoparticles became fluorescent (Scheme 1). This was not unprecedented – recent work by Yang and coworkers has shown that the rigidification of polymer nanoparticles can result in the generation of fluorescence from non-fluorescent components, which they have termed the crosslink-enhanced emission effect (CEE).[20] In these systems, it is hypothesized that fluorescence behavior results from the formation of clusters of electron rich heteroatoms such as nitrogen,[21,22] oxygen[23] or sulfur,[24] however the exact mechanism of the CEE is not yet fully understood.

Fluorescent polymer nanoparticles (sometimes termed polymer dots, or Pdots) are of interest because they may have better toxicity and biodistribution profiles than traditional quantum dots (Qdots), making applications in medical diagnostics and drug delivery more feasible.[20] Pdots based on non-conjugated polymers (NCPdots) are a particular target because they are usually easier to synthesize than conjugated Pdots. However, it has not proved straightforward to synthesize NCPdots in a controllable and reproducible manner. This is because the majority of systems use poorly-defined starting materials (for example modified natural polymers, which have high batch-to-batch variability). Many methods for the production of NCPdots (such as hydrothermal synthesis) also do not lend themselves to systematic studies of the origins of fluorescence by the CEE because the chemical structure of the final products is not known and is difficult to determine.[20] We hypothesized that our A:T based system could represent a solution to both of these problems as it is assembled from well-defined starting materials and the composition can be carefully controlled by altering a number of different parameters, including polymer side chain functionality, A:T ratios, crosslinking density and solvent. We therefore set out to further investigate our NCPdot system, with the hope that an increased understanding of the origins of the CEE will aid in the development and application of this interesting new class of materials.

Experimental Section

Materials and characterization methods

Materials. 2,2'-Azo-bis(isobutyronitrile) (AIBN) was obtained from Molekula and recrystallized from methanol. 2,2'-Azobis[2-(2-imidazolin-2-yl)propane]dihydrochloride (VA-044, Wako), 1-Ethylpiperidine hypophosphite (EPHP, Sigma-Aldrich) were used without further purification. 4-Acryloylmorpholine (NAM) was bought from Aldrich and was purified by vacuum distillation. 2-(((butylthio)carbonothiolyl)thio)propanoic acid, 3-bromopropyl acrylate, 3-benzoylthymine, 9-hexyladenine, $PNAM_{96}$, $PNAM_{96}$-*b*-$PAAm_{19}$ (**PA**) and PNAM96-b-PTAm18 (**PT**) were synthesized as described previously and stored at 4 °C.[9,25,26] The p-silicon (100) wafers were purchased from Sigma-Aldrich and were cut into plates with a size of 10 mm × 10 mm for AFM imaging. Dialysis membranes (MWCO = 3.5 kDa) were purchased from Spectra/Por. DMF, DMSO and other chemicals were obtained from Fisher Chemicals and used without further purification. Dry solvents were obtained by passing over a column of activated alumina using an Innovative Technologies solvent purification system.

^{1}H NMR and ^{13}C NMR spectra were recorded on a Bruker DPX-400 or HD500 spectrometer with DMSO-d_6 or DMF-d_7 as the solvent. The chemical shifts of protons were relative to solvent residues (DMF 8.01 ppm and DMSO 2.50 ppm). For the UV irradiation of the samples, a UPV-1000 crosslinker chamber, equipped with 5 × 8 watt UV dual bipin discharge type tubes that emit within the midrange of the UV spectrum with the maximum intensity at 302 nm was used. UV-vis spectra were recorded on a Perkin-Elmer Lambda 35 UV-vis instrument. Fluorescence spectra were recorded using an Agilent Cary Eclipse fluorescence spectrophotometer. Time correlated single photon counting (TCSPC) was employed to obtain all fluorescence lifetime spectra, using an Edinburgh Instruments FLS920 spectrometer and 375 nm solid state ps diode laser source (PicoQuant) in matched quartz 3.5 mL cells (Starna Cell). Instrument response functions (IRF) were determined from scatter signal solution of Ludox HS-40 colloidal silica (0.01% particles in water wt/wt). Fourier transform infrared (FT-IR) spectra were obtained using a Perkin Elmer Spectrum 100 FT-IR. Scans from 550 to 4000 cm^{-1} were taken, and the spectra corrected for background absorbance. The spectra were normalized to the absorbance at 2000 cm^{-1} for comparison. High resolution mass spectrometry (HR-MS) was conducted on a Bruker UHR-Q-TOF MaXis with electrospray ionization (ESI). HPLC was carried out using XBridgeTM OST C18 (2.5 µm) 50 × 4.6 mm column. The HPLC system was an Agilent 1260 infinity series stack equipped with an Agilent 1260 binary pump, mixer and degasser. Samples were injected using an Agilent 1260 autosampler and detection was achieved using an Agilent 1260 variable wavelength detector, connected in series. UV detection was monitored at λ = 260 nm and the mobile phase used was 100% v/v water. Size exclusion chromatography (SEC) data were obtained in HPLC grade DMF containing 5 mM NH_4BF_4 at 50 °C, with a flow rate of 1.0 mL min^{-1}, on a set of two PLgel 5 µm Mixed-D columns, and a guard column. SEC data were analyzed with Cirrus SEC software calibrated using poly(methyl methacrylate) (PMMA) standards. Preparative SEC was conducted using DMSO at 50 °C, with a flow rate of 0.5 mL min^{-1}.

Hydrodynamic diameters (Dh) and size distributions of the self-assemblies were determined by dynamic light scattering (DLS). The DLS instrumentation consisted of a Malvern Zetasizer NanoS instrument with a 4 mW He-Ne 633 nm laser module. Measurements were made at a detection angle of 173°, and Malvern DTS 7.03 software was used to analyze the data. D_h was calculated by fitting the apparent diffusion coefficient in the Stokes-Einstein equation $D_h = kT/(3\pi\eta D_{app})$, where k, T and η are the Boltzmann constant, the temperature and the viscosity of the solvent, respectively. As the measured sample is a solution of monodispersed spherical micelles, D_h coincides to the real hydrodynamic diameter as D_{app} is equal to the translational diffusion coefficient (D_t). Static light scattering (SLS) measurements were conducted with an ALV CGS3 (λ = 632 nm) at 25 °C. The data were collected from 50° to 130° with an interval of 5°. The self-assembled solutions were filtered through 0.45 µm nylon filters prior to analysis. Small-angle X-ray scattering (SAXS) experiments were performed using Xeuss 2.0 facility. The samples in solutions were run using 1.5 mm diameter quartz capillaries. All patterns were normalized to a fixed transmitted flux using a quantitative beam stop detector. The two-dimensional SAXS images were converted into one-dimensional SAXS profile (I(q) versus q) by circular averaging, where I(q) is the scattering intensity.

TEM observations were performed on a JEOL 2000FX electron microscope at an acceleration voltage of 200 kV. All TEM samples were prepared on graphene-oxide (GO)-coated lacey carbon grids (400 Mesh, Cu, Agar Scientific), to enable high contrast TEM images without any staining.[27] Generally, a drop of sample (10 µL) was pipetted on a grid and left for several minutes, then blotted away. TEM images were analyzed using the ImageJ software, and over 100 particles were counted for each sample to obtain number-average diameter D_n. AFM imaging and analysis were performed on an Asylum Research MFP3D-SA atomic force microscope in tapping mode. Samples for AFM analysis were prepared by drop casting 5 µL of solution (0.1 mg mL^{-1}) onto a freshly clean silicon wafer. The silicon wafer was washed with water and ethanol, then activated using plasma treatment to generate a hydrophilic surface.

Synthetic procedures

Synthesis of 3-(3-methylthymin-1-yl)propyl acrylamide (MTAm)

A mixture of 3-(thymin-1-yl)propyl acrylamide (TAm) (71 mg, 0.3 mmol), dry K_2CO_3 (66 mg, 0.48 mmol), iodomethane (75 µL) in anhydrous DMF (0.4 mL) was stirred at room temperature for 24 h, and then diluted with 20 mL ethyl acetate, washed with water (2 × 20 mL) and dried with anhydrous Na_2SO_4 (Scheme S1). The solvent was removed under vacuum. The mixture was further purified by column chromatography with a mixture of CH_2Cl_2/CH_3OH (95:5) to give a white solid (73 mg, 0.29 mmol, 97%). Overview in Scheme S1. Assigned ^{1}H, ^{13}C NMR spectra are shown in Figure S1. ^{1}H NMR (500 MHz, DMSO-d_6) δ = 8.12 (t, J = 5.0 Hz, CON*H*), 7.59 (s, 1H, pyrimidine-*H*$_6$), 6.18 (dd, J = 17.5, 10.5 Hz, 1H, CH_2=C*H*-CO), 6.07 (dd, J = 17.5, 2.0 Hz, 1H, CH=CH_2-CO), 5.58 (dd, J = 10.5, 2.0 Hz, 1H, CH=CH_2-CO), 3.70 (t, 2H, J = 7.5 Hz, CH_2-pyrimidine), 3.17 (s, 3H, OC-NCH_3), 3.14 (m, 2H, OC-HN-CH_2), 1.80 (s, 3H, CH_3-pyrimidine), 1.76 (m, 2H, OC-NH-CH_2-CH_2-CH_2-pyrimidine) ppm; ^{13}C NMR (125 MHz, DMSO-d_6) δ = 165.1, 163.8, 151.5, 140.4, 132.2, 125.5, 107.9, 47.1, 36.3, 29.0, 28.0, 13.1 ppm; HR-MS (m/z) found 274.1165, calc. 274.1162 $[M+Na]^+$.

Synthesis of 3-(adenine-9-yl)propyl acrylate (AAc)

To a suspension of adenine (3.0 g, 24.2 mmol) in dry DMF (100 mL), NaH (0.85 g, 35.4 mmol) was slowly added (Scheme S2). The mixture was stirred for 1 h until no gas was produced. The viscous mixture was immersed into an ice bath and 3-bromopropyl acrylate freshly synthesized (5.4 g, 28.2 mmol) was added dropwise. The yellow viscous mixture was stirred overnight and the resulting suspension was concentrated under vacuum. The solid was washed with CH_2Cl_2 several times and then concentrated. The mixture was further purified by column chromatography using a mixture of CH_2Cl_2 and CH_3OH as eluent and a gradient from 1:0 to 95:5 to give a white solid, AAc (0.55 g, 9%). Assigned ^{1}H, ^{13}C NMR spectra are shown in Figure S2. ^{1}H NMR (500 MHz, DMSO-d_6) δ = 8.14 (s, 1H, purine *H*-2), 8.12 (s, 1H, purine *H*-8), 7.18 (s, 2H, NH_2), 6.25 (d, J = 17.0 Hz, 1H, CH_2=CH-CO), 6.08 (dd, J = 17.0 Hz, 10.0 Hz, 1H, CH_2=C*H*-CO), 5.91 (d, J = 10.0 Hz, 1H,

CH_2=CH-CO), 4.25 (t, 2H, J =6.5 Hz, CH_2-purine) 4.10 (t, 2H, J =6.0 Hz, OC-O-CH_2), 2.19 (m, 2H, J =6.5 Hz, OC-O-CH$_2$-CH_2-CH$_2$-purine) ppm; ^{13}C NMR (400 MHz, DMSO-d_6) δ = 165.8, 156.4, 152.8, 150.1, 141.3, 132.0, 128.6, 119.2, 62.1, 40.7, 28.9 ppm; HR-MS (m/z) found 270.0961, calc. 270.0962 $[M+Na]^+$.

Synthesis of 3-(3-benzoylthymin-1-yl)propyl acrylate

To the solution of 3-benzoylthymine (4.6 g, 20.0 mmol) in dry DMF (100 mL), NaH (0.50 g, 21.0 mmol) was slowly added (Scheme S3). The mixture was stirred for 1 h until no gas was produced. The viscous mixture was immersed in an ice bath and 3-bromopropyl acrylate freshly synthesized (4.6 g, 24.0 mmol) was added dropwise. The yellow, viscous mixture was stirred overnight. The resulting solution was concentrated under vacuum. The residue was partitioned with EtOAc and water. The aqueous layer was extracted three times with EtOAc and the combined organic layers were dried over anhydrous $MgSO_4$. The solvent was removed under vacuum. The mixture was further purified by column chromatography using EtOAc as eluent to give a viscous liquid (4.2 g, 61%). ^{1}H NMR (400 MHz, DMSO-d_6) δ = 7.93 (d, J = 7.2 Hz, 2H, benzene-*H*1,*H*5), 7.80 (s, 1H, pyrimidine-*H*6), 7.78 (t, J = 7.6 Hz, 1H, benzene-*H*3), 7.59 (t, J = 7.6 Hz, 2H, benzene-*H*2, *H*4), 6.32 (dd, J = 17.2 Hz, 1.6 Hz, 1H, CH_2=CH-CO), 6.14 (dd, J = 17.2 Hz, 10.4 Hz, 1H, CH$_2$=C*H*-CO), 5.94 (dd, J = 10.4 Hz, 1.6 Hz, 1H, CH_2=CH-CO), 4.18 (t, 2H, J = 7.0 Hz, OC-O-CH_2), 3.93 (t, 2H, J = 7.0 Hz, CH_2-pyrimidine), 2.02 (m, 2H, J = 6.4 Hz, OC-O-CH$_2$-CH_2-CH$_2$-pyrimidine), 1.83 (s, 3H, CH_3-pyrimidine) ppm; ^{13}C NMR (400 MHz, DMSO-d_6) δ = 170.2, 165.8, 163.4, 149.9, 143.0, 135.9, 132.1, 131.7, 130.9, 130.0, 128.6, 109.0, 62.3, 46.0, 27.8, 12.3 ppm.

Synthesis of 3-(thymin-1-yl)propyl acrylate (TAc)

(3-Benzoylthymin-1-yl)propyl acrylate (3.0 g, 8.8 mmol) was dissolved in a mixture of TFA/DCM (3:1) (20 mL) (Scheme S3). The reaction solution was stirred at room temperature overnight. After completion of the reaction, solvent was removed under vacuum. The residue was purified by column chromatography with a gradient of $CHCl_3$/CH_3OH from 1:0 to 95:5 to give a viscous liquid. Ethanol (20 mL) was then added to give a white solid (1.70 g, 74%). Assigned ^{1}H, ^{13}C NMR spectra are shown in Figure S3. ^{1}H NMR (500 MHz, DMSO-d_6) δ = 11.21 (s, 1H, pyrimidine-*H*3), 7.52 (s, 1H, pyrimidine-*H*6), 6.30 (d, J = 16.5 Hz, 1H, CH_2=CH-CO), 6.11 (dd, J = 16.5 Hz, 10.0 Hz, 1H, C*H*=CH$_2$-CO), 5.93 (d, J = 10.0 Hz, 1H, CH_2=CH-CO), 4.12 (t, 2H, J = 6.0 Hz, OC-O-CH_2), 3.73 (t, 2H, J = 6.5 Hz, CH_2-pyrimidine), 1.95 (m, 2H, J = 6.5 Hz, OC-O-CH$_2$-CH_2-CH$_2$-pyrimidine), 1.73 (s, 3H, CH_3-pyrimidine) ppm; ^{13}C NMR (500 MHz, DMSO-d_6) δ = 165.8, 164.8, 151.4, 141.9, 132.0, 128.6, 109.0, 62.3, 45.3, 27.9, 12,4 ppm; HR-MS (m/z) found 261.0840, calc. 261.0846 $[M+Na]^+$.

Synthesis of PNAM$_{96}$-*b*-PMTAm$_{19}$ (PT$^{Me'}$), PNAM$_{96}$-*b*-PAAc$_{20}$ (PA*') and PNAM$_{96}$-*b*-PTAc$_{19}$ (PT*') diblock copolymers

The typical procedure was as follows. For PNAM$_{96}$-*b*-PMTAm$_{19}$ (**PT$^{Me'}$**), PNAM$_{96}$ (69 mg, 0.005 mmol), MTAm (25 mg, 0.1 mmol), and AIBN (0.08 mg, 0.0005 mmol) were dissolved in DMSO (0.3 mL). The mixture was thoroughly degassed via 4 freeze-pump-thaw cycles, filled with nitrogen and then immersed in an oil bath at 70 °C overnight. An aliquot of the crude product was taken and analyzed by ^{1}H NMR spectroscopy to calculate the conversion. The residual solution was precipitated three times from cold CH_3OH. The light yellow polymer was dried in a vacuum oven overnight at room temperature and analyzed by ^{1}H NMR spectroscopy and DMF SEC.

End group removal of PNAM$_{96}$-*b*-PAAm$_{19}$ (PA'), PNAM$_{96}$-*b*-PTAm$_{18}$ (PT'), PNAM$_{96}$-*b*-PMTAm$_{19}$ (PT$^{Me'}$), PNAM$_{96}$-*b*-PAAc$_{20}$ (PA*') and PNAM$_{96}$-*b*-PTAc$_{19}$ (PT*') diblock copolymers

The typical procedure was as follows. PNAM$_{96}$-b-PAAm$_{19}$ (**PA'**) (100 mg, 0.0052 mmol), EPHP (9.4 mg, 0.052 mmol), and AIBN (0.28 mg, 0.0017 mmol) were dissolved in DMF (2.0 mL) (Scheme S4). The mixture was thoroughly degassed via 4 freeze-pump-thaw cycles, filled with nitrogen and then immersed in an oil bath at 100 °C for 2 h. The solution was precipitated three times from cold CH_3OH. The diblock copolymer was further purified by dialysis against 18.2 MΩ·cm water (MWCO = 3.5 kDa), incorporating at least 6 water changes and followed by lyophilization to yield a white solid. The obtained white polymer **PA** was further analyzed by ^{1}H NMR spectroscopy and DMF SEC (Figures S4-S5 and Table S1).

Self-assembly and UV irradiation of micelles MA, MT, M(A:T), M(A+T^{Me}), M(A*:T*) and Mi(9-hexylA:T)

The typical procedure was as follows. For **M(A:T)**, diblock copolymers **PA** (10 mg, 0.00052 mmol) and **PT** (10 mg, 0.00052 mmol) were dissolved in H_2O (2.0 mL). The obtained solution was kept stirring for at least 2 h at room temperature prior to use. The self-assembled solution was then transferred to an NMR tube for UV irradiation using a UPV-1000 crosslinker chamber.

Hydrolysis of micelles Mi(A:T) and Mi(A*:T*)

The typical procedure was as follows. **Mi(A*:T*)** (10 mg) was dissolved using 1 M HCl aqueous solution (1 mL) and was kept stirring at room temperature for 7 days. Then 1 M $NaHCO_3$ aqueous solution was added to tune the pH to 7. The mixture was passed through neutral Al_2O_3 column and the solvent was removed under vacuum and the obtained white solid was characterized using DMF SEC and fluorescence spectrophotometer. In order to further analyze the hydrolyzed products in **MiH(A*:T*)**, the solution was dialyzed (MWCO = 3.5 kDa). The dialyzate was freeze-dried and analyzed by HPLC and HR-MS.

Results & Discussion

For our initial experiments, two diblock copolymers with short nucleobase core-forming blocks, poly(4-acryloylmorpholine)-*b*-poly(3-(adenine-9-yl)propyl acrylamide) (PNAM-*b*-PAAm) and poly(4-acryloylmorpholine)-*b*-poly(3-(thymin-1-yl)propyl acrylamide) (PNAM-*b*-PTAm) were prepared and the trithiocarbonate end group removed as described previously (Figures S4-S5).[9,28] The resulting diblock copolymers, PNAM$_{96}$-*b*-PAAm$_{19}$ (**PA**; with a hydrophobic adenine block) and PNAM$_{96}$-*b*-PTAm$_{18}$ (**PT**; with a hydrophobic thymine block) were mixed in a 1:1 molar ratio and self-assembled by direct dissolution in water at 10 mg mL^{-1} to give micelles **M(A:T)**, which were characterized by static and dynamic light scattering (SLS and DLS) (Figures S6-S8). We attempted characterization by transmission electron microscopy (TEM), but the particles disassembled upon drying to give a polymer film. **M(A:T)** were then irradiated with UV light at 302 nm for 12 h (*ca.* 170 J cm^{-2}) to form nanoparticles **Mi(A:T)** as shown in Scheme 1. TEM indicated that well-defined spherical micelles with a number-average diameter of 13 ± 2 nm were obtained (Figure 1a).

Atomic force microscopy (AFM) studies also confirmed the formation of well-defined nanoparticles (Figure S9). DLS (Figure 1b), SLS and small-angle X-ray scattering (SAXS) analyses showed that no significant change in particle dispersity or size occurred upon irradiation (Figures S6 and S8). Interestingly, **Mi(A:T)** were observed to fluoresce under UV light (Figure 1c). We decided to investigate the causes of this fluorescence behavior by exploiting the tunability of the micelle system.

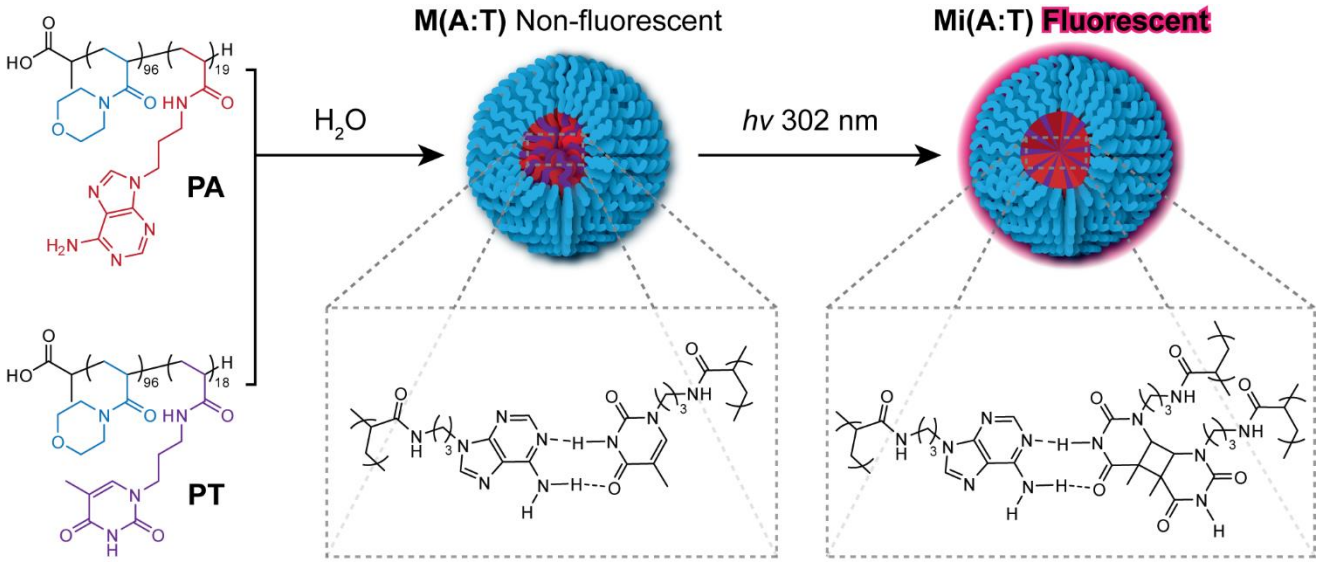

Scheme 1. Synthesis of fluorescent nanoparticles by self-assembly and photocrosslinking of nucleobase-containing polymers. **PA** and **PT** were mixed in a 1:1 molar ratio and dissolved in water, to give micelles **M(A:T)** with complementary A:T base pairing in the core. Irradiation with UV light for 12 hours induced photodimerization of T and yielded fluorescent nanoparticles **Mi(A:T)**.

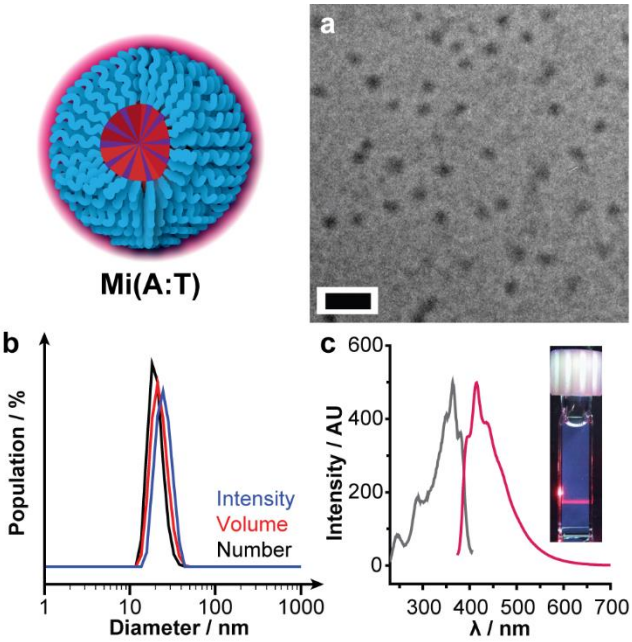

Figure 1. Characterization of the crosslinked nanoparticles **Mi(A:T)**: a) TEM on graphene oxide[27] (scale bar 50 nm); b) DLS analyses by scattered light intensity (blue), particle volume (red) and particle number (black); c) Fluorescence excitation (λ_{em} = 415 nm) and emission (λ_{ex} = 365 nm) spectra (inset **Mi(A:T)** solution under UV lamp (365 nm) with a red laser flux in the horizontal direction).

Effect of H-bonding

We began by exploring whether H-bonding was required for the fluorescence behavior to arise. **PA** and **PT** were self-assembled separately to give micelles **MA** and **MT** respectively, using an identical procedure to that described above for **M(A:T)**. TEM and light scattering analyses confirmed the formation of well-defined micelles (Figures S11-S12), neither of which exhibited significant fluorescence. Irradiation of these micelles gave **MiA** and **MiT**, with no significant changes in particle size or dispersity detected (Figures S11-S12). Again, neither of these was found to exhibit significant fluorescence (Figure 2), supporting the conclusion that A:T H-bonding was indeed important in the generation of fluorescence in this system.

We also investigated an analogue to **Mi(A:T)** in which H-bonding had been disrupted. This was achieved by synthesizing a new monomer in which the T residue had been methylated, and polymerizing as described above to give a methylated version of **PT**, termed $\mathbf{PT^{Me}}$. $\mathbf{PT^{Me}}$ was mixed in a 1:1 molar ratio with **PA** and self-assembled into micelles $\mathbf{M(A+T^{Me})}$, then irradiated to produce $\mathbf{Mi(A+T^{Me})}$. Well-defined particles were observed to form (Figures S13-S14) and neither sample displayed significant fluorescence (Figure 2), so it was concluded that A:T H-bonding was essential for this behavior to arise.

Importance of crosslinking

Next, we set out to confirm that the nanoparticles had indeed been crosslinked by the irradiation process, by transferring them into DMF, a good solvent for both polymer blocks. Uncrosslinked micelles were expected to disassemble into the component polymers under these conditions, whereas crosslinked nanoparticles were anticipated to survive largely intact (Figure 3). **MA**, **MT**, **M(A:T)**, **MiA**, **MiT** and **Mi(A:T)** were all transferred from water to DMF and analyzed by size exclusion chromatography (SEC, eluting with DMF). All uncrosslinked micelles (**MA**, **MT** and **M(A:T))** were found to exhibit a single peak, the mass of which was consistent with the constituent free polymers (**PA** and/or **PT**), see Figure 3 (black/gray traces). The irradiated micelles **MiA**, which contained no thymine groups and were therefore not expected to crosslink under UV light, also eluted as a single peak with the same mass as **PA** (Figure 3a, red traces). In contrast, **MiT** and **Mi(A:T)** exhibited a new peak at around 250 kDa, which was attributed to crosslinked nanoparticles that were incapable of disassembly in DMF (Figure 3b and c, purple and pink traces respectively). Based on these data, it was concluded that the nanoparticles were indeed highly crosslinked, and the lack of any significant fluorescence for **MiT** confirmed that crosslinking was necessary but not sufficient for fluorescence to arise.

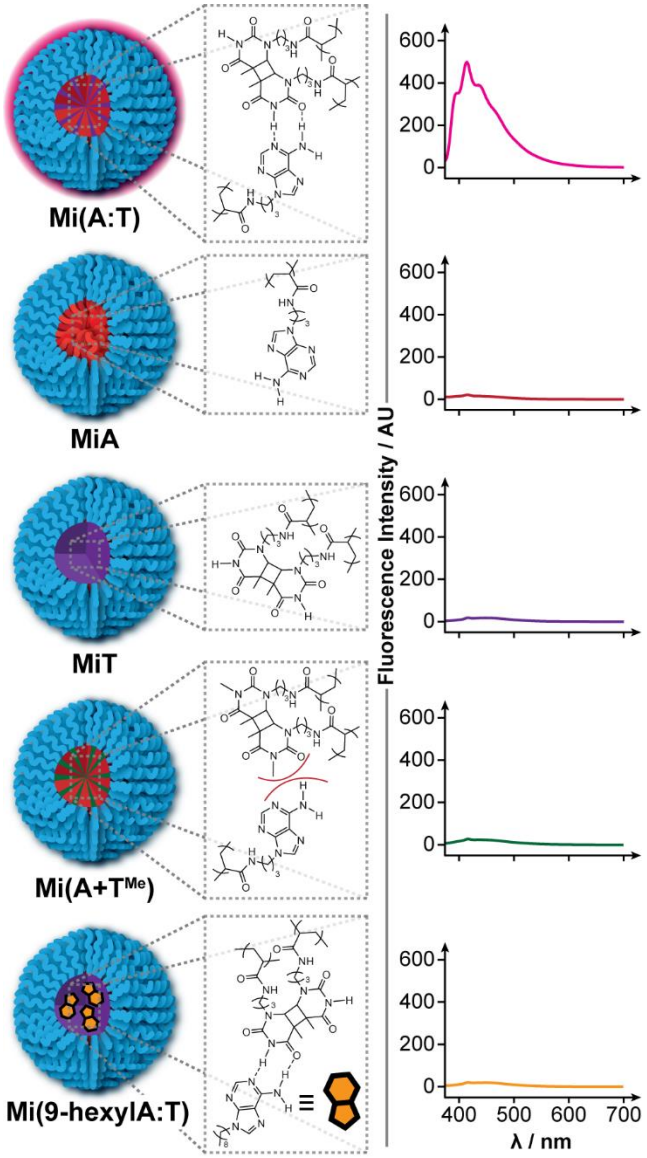

Figure 2. Cartoons showing the core compositions of irradiated micelles **Mi(A:T)**, **MiA**, **MiT**, **Mi(A+T^{Me})** and **Mi(9-hexylA:T)**, and (right) fluorescence emission spectra (λ_{ex} = 365 nm) for these particles, showing that no significant fluorescence was observed as a result of the absence or interruption of H-bonding, or detachment of A from the polymer backbone.

Requirement for polymer immobilization

To test whether immobilization of A on a polymer backbone was necessary for fluorescence behavior, we assembled **PT** in the presence of 1 molar equivalent of 9-hexyladenine (**9-hexylA**) to form micelles **M(9-hexylA:T)**, which were subsequently irradiated to give nanoparticles **Mi(9-hexylA:T)** (Figure 2 and S16-S17). Interestingly, this system was not fluorescent, so we concluded that immobilization of A by attachment to a polymer backbone was also essential for the CEE to occur. This further suggested that rigidification of the polymer nanoparticle was key in the generation of fluorescence.

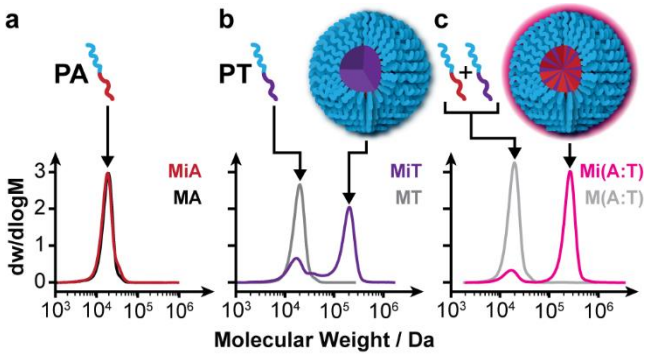

Figure 3. SEC traces using DMF as solvent of (a) **MA** and **MiA**; (b) **MT** and **MiT**; (c) **M(A:T)** and **Mi(A:T)**. In cases where T was present in the core, a new peak at around 250 kDa appeared, attributed to the crosslinked nanoparticles, which could not disassemble even in a good solvent.

Probing the crosslinking process

We studied the crosslinking process using spectroscopy in order to gain further insights into the generation of fluorescence in our system. **MA**, **MT** and **M(A:T)** were each irradiated for a total of twelve hours, with aliquots removed at regular time intervals for analysis by UV-vis and fluorescence spectroscopy (at 0.1 mg mL^{-1}). As expected, a gradual decrease in absorbance at 272 nm, was observed for **MiT** and **Mi(A:T)**, which was attributed to the photodimerization of thymine (Figure 4a). As no obvious alterations were observed in the spectra of **MiA** after UV irradiation (Figure S21a), we could quantify the thymine photodimerization degree using the decrease in absorbance at 272 nm during UV irradiation. The crosslinking of thymine in both **MiT** and **Mi(A:T)** appeared to be very efficient (Figure S22) with around 90% photodimerization achieved after 12 h irradiation, which was consistent with the SEC results described above. Fluorescence spectroscopy of the irradiated solution of **M(A:T)** revealed an increase in fluorescence over the course of the crosslinking experiment as expected (Figure 4b).

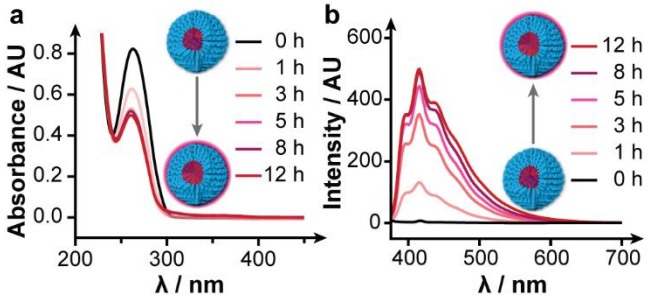

Figure 4. UV-vis absorption (a) and fluorescence emission (b, λ_{ex} = 365 nm) spectra of **M(A:T)** after different irradiation times to form **Mi(A:T)**, showing the decrease in absorbance at 272 nm due to crosslinking of the T groups and the appearance of the characteristic fluorescence peak for the crosslinked nanoparticles.

By combining the UV-vis and fluorescence measurements for irradiation of **M(A:T)**, it was possible to plot fluorescence intensity versus degree of crosslinking (Figure 5). Interestingly, this revealed a non-linear relationship: at a critical point (around 3h irradiation time, or approximately 80% thymine photodimerization) a notable increase in fluorescence was observed. This suggested that a certain minimum degree of crosslinking was required in order for the CEE to emerge and cause fluorescence.

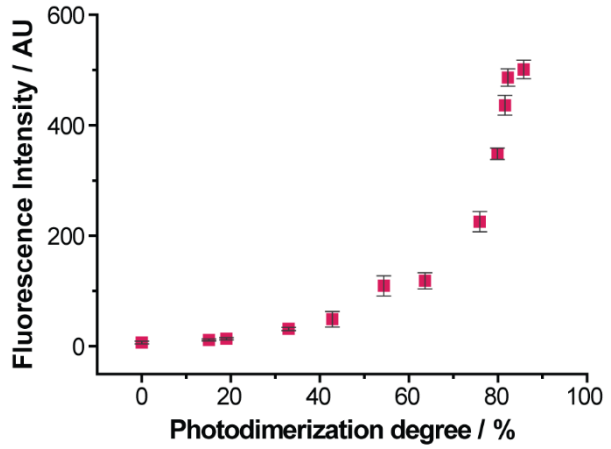

Figure 5. Plot of fluorescence intensity at 415 nm *versus* photodimerization degree showing the non-linear relationship. Error bars are the standard deviation from three experimental replicates.

During the UV-vis experiments we observed a small tail above 300 nm in the UV-vis absorption spectrum , which developed at prolonged irradiation times. However, due to the relatively low concentration, no recognizable features could be determined. Irradiation of **M(A:T)** at a much higher concentration (9.5 mg mL^{-1}) was therefore investigated. Three peaks at 346, 362 and 380 nm were initially observed after 3 h of UV irradiation followed by a smooth increase in intensity (Figure 6). When both **M(A:T)** and **Mi(A:T)** were excited at 305 nm, **M(A:T)** showed no obvious emission and **Mi(A:T)** showed decreased emission but with a characteristic triple peak pattern. This result supports the observed fluorescence emission originates from the species absorbing at 365 nm. Notably, the same features were not observed during irradiation of **MA** or **MT**, suggesting that the interaction between complementary nucleobases in the crosslinked core played an important part in generating them. In agreement with the fluorescence spectroscopy results above, a plot of UV absorbance at 362 nm versus photodimerization degree displayed a non-linear relationship (Figure S23). This further supported the conclusion that a certain critical amount of crosslinking was required to induce fluorescence.

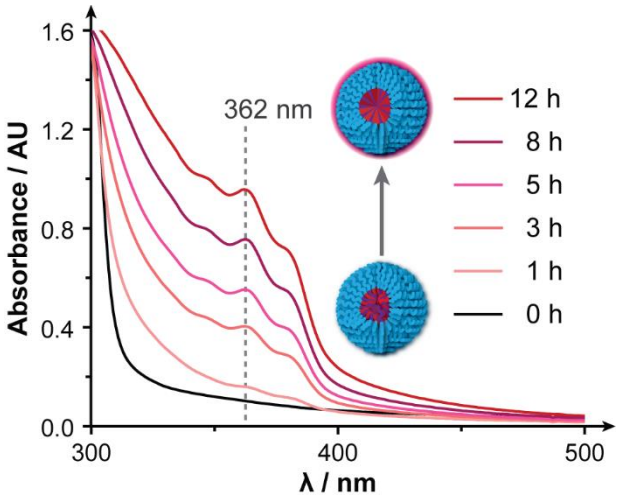

Figure 6. UV-vis absorption spectrum of **M(A:T)** after different irradiation times to form **Mi(A:T)** at a higher concentration of 9.5 mg mL^{-1} showing the appearance of vibronic features with a principle peak at 362 nm.

Characterization of fluorescence pathways

In order to provide further information about the nature of the fluorophore created in **Mi(A:T)**, solution-state time-correlated single-photon counting (TCSPC) was conducted to determine the fluorescence lifetimes of the constructs (Figure 7 and Table S2). For samples which contained adenine – **Mi(A:T)**, **MiA** and **M(A:T)** – TCSPC measured at λ_{em} = 415 nm showed almost identical emission decay profiles once the significant difference in the signal to noise ratio between **Mi(A:T)** and the other two samples was taken into account. Moreover, all three adenine-containing samples shared the same two longer lifetime components (τ_2 = ~4 ns and τ_3 = ~11 ns; see Table S2 for details). However, whilst the aforementioned lifetimes were in agreement, there were marked differences in the fluorescence quantum yields (QY). The relative QY of **Mi(A:T)** was 7.9% (Table S3) (comparable to that of quantum carbon dots[29]), which was 80-fold higher than that of **M(A:T)** and 40-fold higher than that of **MiA**. These results suggested that rather than creating a new fluorophore, crosslinking resulted in the promotion of an already extant emissive pathway. Without crosslinking, the initially populated state (with a lifetime shorter than the TCSPC instrument response) was able to decay via alternative, non-emissive, pathways to the ground state. Crosslinking resulted in a higher fraction of the initially populated state passing into the emissive pathway, likely promoted by π–π stacking,[30,31] and hence increased fluorescence.

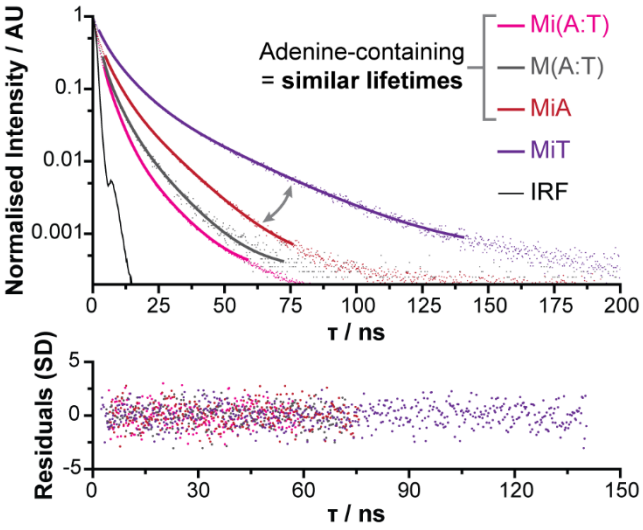

Figure 7. Normalized TCSPC fluorescence lifetime decay spectra with residuals for **MiA**, **MiT**, **M(A:T)** and **Mi(A:T)** in water at 0.5 mg mL^{-1}, showing the similarity between the adenine-containing samples. The instrument response function (IRF, black) is also shown for comparison.

Degradation Studies

In order to rule out the possibility that the observed fluorescence was due to the formation of new molecular species (other than the thymine dimer) during irradiation, an additional crosslinked mixed micelle **Mi(A*:T*)** was prepared (Figure 8). This micelle was analogous to **Mi(A:T)** (and showed similar fluorescence properties, see Figure 8c) but it contained a hydrolyzable ester rather than a stable amide linkage between the nucleobase and polymer backbone, to allow for nanoparticle disassembly. The acrylate-containing nanoparticles **Mi(A*:T*)**, were hydrolyzed in 1 M HCl aqueous solution at room temperature for 7 days to form **MiH(A*:T*)** and then the polymer and small molecules were separated by dialysis. SEC and NMR analyses of the high molecular weight product confirmed successful cleavage of the nucleobase functionalities and the presence of poly(4-acryloylmorpholine)-b- poly(acrylic acid) (PNAM-

b-PAA) (Figure 8b and Figure S25). A loss of fluorescence of the solution of **MiH(A*:T*)** was observed compared to the parent micelle **Mi(A*:T*)**, as shown in Figure 8c. The small molecules were analyzed by HPLC which revealed the presence of 2 species (Figure 8d), neither of which were fluorescent. The species at 4.5 min had a strong UV peak absorption at 260 nm which was confirmed by MS

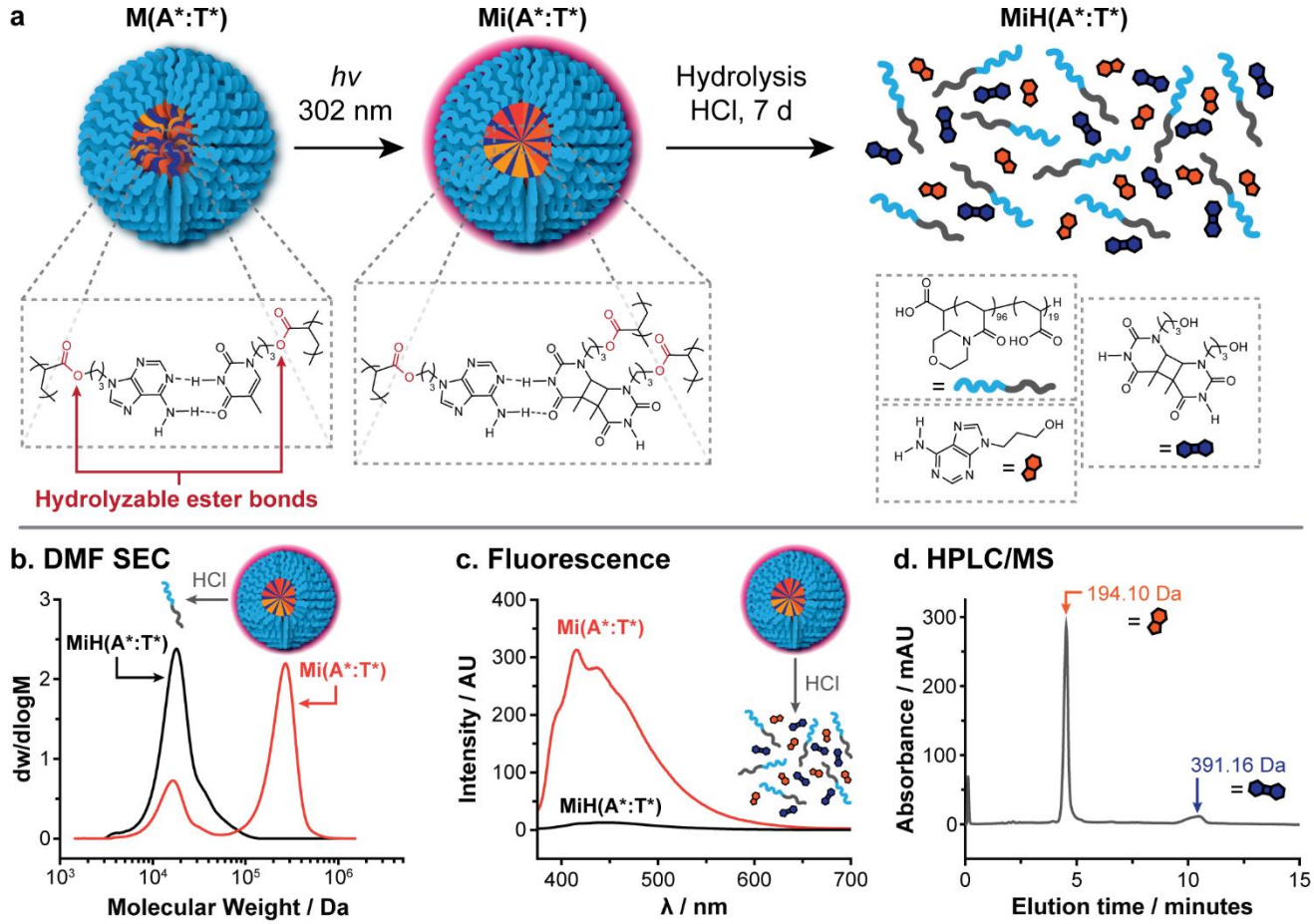

Figure 8. Synthesis and characterization of the hydrolyzable nanoparticle **Mi(A*:T*):** a) cartoon illustrating the crosslinking and subsequent disassembly of **Mi(A*:T*)** by hydrolysis to give **MiH(A*:T*)**; b) DMF SEC analysis of **Mi(A*:T*)** showing the persistent high molecular weight peak attributed to the crosslinked nanoparticle (orange trace) – following hydrolysis to produce **MiH(A*:T*)** (black trace) this peak disappeared and the trace indicated only the presence of free polymer; c) Fluorescence emission spectra (λ_{ex} = 365 nm) of **Mi(A*:T*)** and **MiH(A*:T*)** showing the loss of fluorescence upon hydrolysis; d) HPLC chromatogram showing the two low molecular weight species isolated upon hydrolysis of **Mi(A*:T*)** – MS analyses (shown above each peak) confirmed these to be the expected products.

to be attributable to adenine moieties and the second species at longer retention time was attributed to the thymine dimer (Figure 8d). As a control reaction the stable acrylamide crosslinked micelle, **Mi(A:T)**, was reacted under the same conditions and no obvious hydrolysis (as determined by SEC) or loss in fluorescence occurred (Figure S26).

Robustness to changes in temperature, solvent and pH

We were also interested in exploring the response of **Mi(A:T)** to changes in temperature, solvent and pH. The fluorescence of both **M(A:T)** and **Mi(A:T)** was unchanged after heating at 60 °C overnight, indicating stable fluorescent properties (Figure S27). Luminogens based on aggregation-induced emission are traditionally formed *via* the solvophobic effect and are therefore not very robust towards such changes;[32] we speculated that our highly crosslinked nanoparticles may be more resistant. **Mi(A:T)** was dissolved in a series of solvents of different polarities (Figure 9a). Complete quenching of the fluorescence was not observed in any of the solvents tested but there was a variation in emission intensity, which correlated with the differing abilities of the solvents to solvate/swell the micelle core and disrupt A:T interactions. To further test this hypothesis, we examined the drop in fluorescence when nanoparticles with lower crosslink densities were dissolved in DMF and DMSO (Figure S28). A greater percentage drop in fluorescence was observed at lower crosslink densities, which we attributed to the increased ability of the solvents to penetrate into the core and disrupt the fluorophore.

Finally, we investigated the effect of changing the solution pH. **Mi(A:T)** was dissolved in buffers at different pH and the fluorescence intensity measured (Figure 9b). Almost no change in intensity was recorded across the pH range used, with the exception of pH 2, which we speculated may be due to protonation of adenine.[33] Meanwhile, no impact on fluorescence was observed with a range of NaCl concentrations present, underscoring the system's potential for biomedical applications (Figure S29).

Conclusions

Based on the data presented above, we propose that the fluorescence of the **Mi(A:T)** nanoparticles arises because of the entrapment and rigidification of adenine by the photocrosslinked thymine network. Under these conditions, adenine units are forced into a particular configuration that favors the population of an emissive decay pathway. Based on literature reports on the excited state dynamics of oligonucleotides,[30,31] it seems reasonable to suggest that π–π stacking drives this process. This interpretation is supported by the observation that any change to the system that results in a less ordered and tightly packed nanoparticle core – interruption of H-bonding, absence of crosslinking, detachment of the nucleobase from the polymer backbone – results in fluorescence effectively being switched off. We could find no evidence, either through TCSPC or degradation studies, that any new molecular species are formed during the crosslinking process, which provides further support for the conclusion that fluorescence is induced by aggregation of usually non-fluorescent components. The hypothesis that rigidification is responsible for fluorescence is supported by the distinct vibronic bands in the UV-vis absorption and fluorescence spectra of **Mi(A:T)** (Figure 6 and Figure 1c), which are characteristic of the formation of rigid structures.[34]

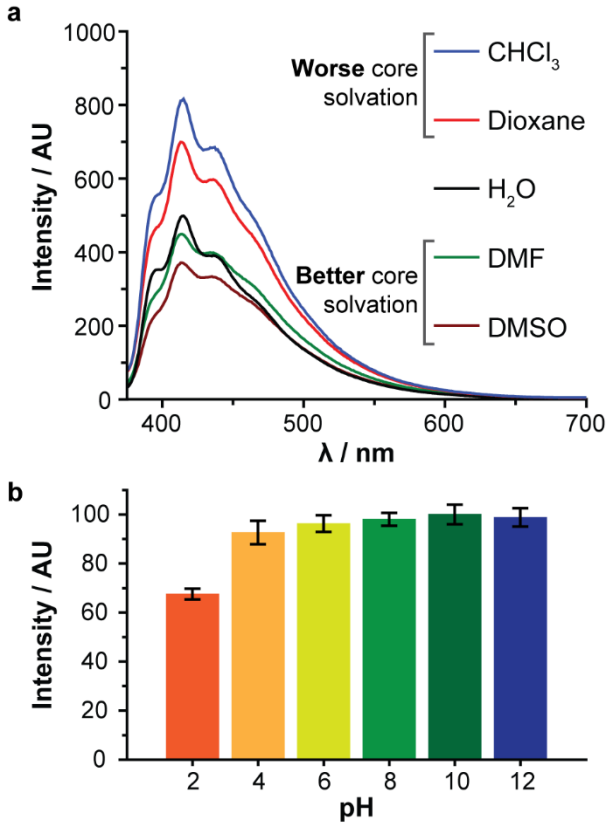

Figure 9. Effect of solvent conditions on **Mi(A:T)** fluorescence: a) Fluorescence emission spectra (λ_{ex} = 365 nm) for **Mi(A:T)** dispersed in different solvents; b) Dependence of fluorescence emission intensity at 415 nm (λ_{ex} = 365 nm) on aqueous solution pH for **Mi(A:T)** – data were scaled so that the emission intensity at pH 10 was 100 AU.

Taken together, these data confirm the formation of a new class of NCPdot based on synergistic chemical crosslinking and selective H-bonding. By assembling the NCPdots out of well-defined polymer components, it was possible to selectively change the make-up of the nanoparticles in order to tease apart the underlying fluorescence mechanism. We propose that this could provide a general strategy for understanding the mechanisms underpinning the CEE.

NCPdots that possess core-shell structures could offer a number of advantages over classical fluorescent organic dyes. Most notably, the corona/shell can provide an effective physical shield from complicated exterior environments, resulting in more stable fluorescence – our investigations into the effects of different solvents and pHs provide a tentative first proof of this concept. We also anticipate that it may be possible to generalize our strategy to create a diverse array of new NCPdots by combining selective supramolecular interactions with chemical crosslinking. This possibility is currently under investigation in our laboratory.

ASSOCIATED CONTENT

Supporting information

Characterization data, further microscopy images, spectroscopy. This material is available free of charge via the Internet at http://pubs.acs.org.

AUTHOR INFORMATION

Corresponding Author

* rachel.oreilly@warwick.ac.uk

Author Contributions

The manuscript was written through contributions of all authors.

Funding Sources

The authors thank the University of Warwick, China Scholarship Council (Z. H.), EPSRC, The Royal Society, The Leverhulme Trust and the ERC (grant number 615142) for research funding.

ACKNOWLEDGMENTS

Drs. Jeffery Foster and Wendong Quan are thanked for helpful discussions. Drs. Zoe Pikramenou and Steve Huband are also thanked for help with the fluorescence lifetime and SAXS measurements, respectively.

REFERENCES

(1) South, C. R.; Weck, M. Template-Enhanced Ring-Opening Metathesis Polymerization. *Macromolecules* **2007**, *40*, 1386–1394.

(2) Lo, P. K.; Sleiman, H. F. Nucleobase-Templated Polymerization: Copying the Chain Length and Polydispersity of Living Polymers into Conjugated Polymers. *J. Am. Chem. Soc.* **2009**, *131*, 4182–4183.

(3) Gorska, K.; Winssinger, N. Reactions Templated by Nucleic Acids: More Ways to Translate Oligonucleotide-Based Instructions into Emerging Function. *Angew. Chem. Int. Ed.* **2013**, *52*, 6820–6843.

(4) O'Reilly, R. K.; Turberfield, A. J.; Wilks, T. R. The Evolution of DNA-Templated Synthesis as a Tool for Materials Discovery. *Acc. Chem. Res.* **2017**, *50*, 2496–2509.

(5) McHale, R.; Patterson, J. P.; Zetterlund, P. B.; O'Reilly, R. K. Biomimetic Radical Polymerization via Cooperative Assembly of Segregating Templates. *Nat. Chem.* **2012**, *4*, 491–497.

(6) McHale, R.; OReilly, R. K. Nucleobase Containing Synthetic Polymers: Advancing Biomimicry via Controlled Synthesis and Self-Assembly. *Macromolecules* **2012**, *45*, 7665–7675.

(7) Lutz, J. F.; Thünemann, A. F.; Rurack, K. DNA-like "Melting" of Adenine- and Thymine-Functionalized Synthetic Copolymers. *Macromolecules* **2005**, *38*, 8124–8126.

(8) Ilhan, F.; Galow, T. H.; Gray, M.; Clavier, G.; Rotello, V. M. Giant Vesicle Formation through Self-Assembly of Complementary Random Copolymers. *J. Am. Chem. Soc.* **2000**, *122*, 5895–5896.

(9) Hua, Z.; Pitto-Barry, A.; Kang, Y.; Kirby, N.; Wilks, T. R.; O'Reilly, R. K. Micellar Nanoparticles with Tuneable Morphologies through Interactions between Nucleobase-Containing Synthetic Polymers in Aqueous Solution. *Polym. Chem.* **2016**, *7*, 4254–4262.

(10) Hua, Z.; Keogh, R.; Li, Z.; Wilks, T. R.; Chen, G.; O'Reilly, R. K.

Reversibly Manipulating the Surface Chemistry of Polymeric Nanostructures via a "Grafting To" Approach Mediated by Nucleobase Interactions. *Macromolecules* **2017**, *50*, 3662–3670.
(11) Chien, M. P.; Rush, A. M.; Thompson, M. P.; Gianneschi, N. C. Programmable Shape-Shifting Micelles. *Angew. Chem. Int. Ed.* **2010**, *49*, 5076–5080.
(12) Cheng, S.; Zhang, M.; Dixit, N.; Moore, R. B.; Long, T. E. Nucleobase Self-Assembly in Supramolecular Adhesives. *Macromolecules* **2012**, *45*, 805–812.
(13) Beukers, R.; Berends, W. Isolation and Identification of the Irradiation Product of Thymine. *Biochim. Biophys. Acta* **1960**, *41*, 550–551.
(14) Rauer, C.; Nogueira, J. J.; Marquetand, P.; González, L. Cyclobutane Thymine Photodimerization Mechanism Revealed by Nonadiabatic Molecular Dynamics. *J. Am. Chem. Soc.* **2016**, *138*, 15911–15916.
(15) Ishikawa, N.; Furutani, M.; Arimitsu, K. Adhesive Materials Utilizing a Thymine-Adenine Interaction and Thymine Photodimerization. *ACS Macro Lett.* **2015**, *4*, 741–744.
(16) Saito, K.; Ingalls, L. R.; Lee, J.; Warner, J. C. Core-Bound Polymeric Micellar System Based on Photocrosslinking of Thymine. *Chem. Commun.* **2007**, *0*, 2503–2505.
(17) Johnston, P.; Braybrook, C.; Saito, K. Topochemical Photo-Reversible Polymerization of a Bioinspired Monomer and Its Recovery and Repolymerization after Photo-Depolymerization. *Chem. Sci.* **2012**, *3*, 2301–2306.
(18) Kang, Y.; Pitto-Barry, A.; S. Rolph, M.; Hua, Z.; Hands-Portman, I.; Kirby, N.; O'Reilly, R. K. Use of Complementary Nucleobase-Containing Synthetic Polymers to Prepare Complex Self-Assembled Morphologies in Water. *Polym. Chem.* **2016**, *7*, 2836–2846.
(19) Fong, D.; Hua, Z.; Wilks, T. R.; O'Reilly, R. K.; Adronov, A. Dispersion of Single-Walled Carbon Nanotubes Using Nucleobase-Containing Poly(acrylamide) Polymers. *J. Polym. Sci. Part A Polym. Chem.* **2017**, *55*, 2611–2617.
(20) Zhu, S.; Song, Y.; Shao, J.; Zhao, X.; Yang, B. Non-Conjugated Polymer Dots with Crosslink-Enhanced Emission in the Absence of Fluorophore Units. *Angew. Chem. Int. Ed.* **2015**, *54*, 14626–14637.
(21) Sun, B.; Zhao, B.; Wang, D.; Wang, Y.; Tang, Q.; Zhu, S.; Yang, B.; Sun, H. Fluorescent Non-Conjugated Polymer Dots for Targeted Cell Imaging. *Nanoscale* **2016**, No. 8, 9837–9841.
(22) Sun, M.; Hong, C. Y.; Pan, C. Y. A Unique Aliphatic Tertiary Amine Chromophore: Fluorescence, Polymer Structure, and Application in Cell Imaging. *J. Am. Chem. Soc.* **2012**, *134*, 20581–20584.
(23) Gong, Y.; Tan, Y.; Mei, J.; Zhang, Y.; Yuan, W.; Zhang, Y.; Sun, J.; Tang, B. Z. Room Temperature Phosphorescence from Natural Products: Crystallization Matters. *Sci. China Chem.* **2013**, *56*, 1178–1182.
(24) Li, W.; Wu, X.; Zhao, Z.; Qin, A.; Hu, R.; Tang, B. Z. Catalyst-Free, Atom-Economic, Multicomponent Polymerizations of Aromatic Diynes, Elemental Sulfur, and Aliphatic Diamines toward Luminescent Polythioamides. *Macromolecules* **2015**, *48*, 7747–7754.
(25) Barlow, T. R.; Brendel, J. C.; Perrier, S. Poly(Bromoethyl Acrylate): A Reactive Precursor for the Synthesis of Functional RAFT Materials. *Macromolecules* **2016**, *49*, 6203–6212.
(26) Kang, Y.; Pitto-Barry, A.; Maitland, A.; O'Reilly, R. K. RAFT Dispersion Polymerization: A Method to Tune the Morphology of Thymine-Containing Self-Assemblies. *Polym. Chem.* **2015**, *6*, 4984–4992.
(27) Patterson, J. P.; Sanchez, A. M.; Petzetakis, N.; Smart, T. P.; Epps, III, T. H.; Portman, I.; Wilson, N. R.; O'Reilly, R. K. A Simple Approach to Characterizing Block Copolymer Assemblies: Graphene Oxide Supports for High Contrast Multi-Technique Imaging. *Soft Matter* **2012**, *8*, 3322–3328.
(28) Chong, Y. K.; Moad, G.; Rizzardo, E.; Thang, S. H. Thiocarbonylthio End Group Removal from RAFT-Synthesized Polymers by a Radical-Induced Process. *Macromolecules* **2007**, *40*, 4446–4455.
(29) Sun, Y. P.; Zhou, B.; Lin, Y.; Wang, W.; Fernando, K. A. S.; Pathak, P.; Meziani, M. J.; Harruff, B. A.; Wang, X.; Wang, H.; Luo, P. G.; Yang, H.; Kose, M. E.; Chen, B.; Veca, L. M.; Xie, S. Y. Quantum-Sized Carbon Dots for Bright and Colorful Photoluminescence. *J. Am. Chem. Soc.* **2006**, *128*, 7756–7757.
(30) Crespo-Hernández, C. E.; Cohen, B.; Kohler, B. Base Stacking Controls Excited-State Dynamics in A·T DNA. *Nature* **2005**, *436*, 1141–1144.
(31) Su, C.; Middleton, C. T.; Kohler, B. Base-Stacking Disorder and Excited-State Dynamics in Single-Stranded Adenine Homo-Oligonucleotides. *J. Phys. Chem. B* **2012**, *116*, 10266–10274.
(32) Hu, R.; Leung, N. L. C.; Tang, B. Z. AIE Macromolecules: Syntheses, Structures and Functionalities. *Chem. Soc. Rev.* **2014**, *43*, 4494–4562.
(33) Boulard, Y.; Cognet, J. A. H.; Gabarro-Arpa, J.; Le Bret, M.; Sowers, L. C.; Fazakerley, G. V. The pH Dependent Configurations of the C.A Mispair in DNA. *Nucleic Acids Res.* **1992**, *20*, 1933–1941.
(34) Ardoña, H. A. M.; Kale, T. S.; Ertel, A.; Tovar, J. D. Nonresonant and Local Field Effects in Peptidic Nanostructures Bearing Oligo(*p*-Phenylenevinylene) Units. *Langmuir* **2017**, *33*, 7435–7445.

Fluorescent Polymer Nanoparticles

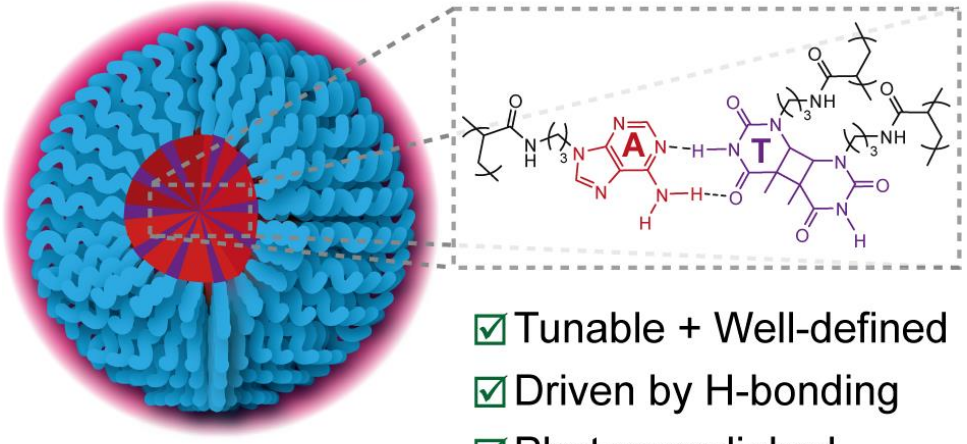

- ☑ Tunable + Well-defined
- ☑ Driven by H-bonding
- ☑ Photocrosslinked